Functional Composite Materials

RESEARCH

Open Access

# Superhydrophobic micro-nanofibers from PHBV-$SiO_2$ biopolymer composites produced by electrospinning

Saad Rabbani*, Reza Jafari and Gelareh Momen

**Abstract**

Electrospinning is a relatively simple technique for producing continuous fibers of various sizes and morphologies. In this study, an intrinsically hydrophilic poly(3-hydroxybutarate-*co*-3-hydroxyvalerate) (PHBV) biopolymer strain was electrospun from a solution under optimal processing conditions to produce bilayers of beadless micro-fibers and beaded nano-fibers. The fibrous mats produced from the pure PHBV solution exhibited hydrophilicity with complete wetting. Incorporation of polydimethylsiloxane (PDMS) treated silica into the electrospinning solutions resulted in a non-wetting state with increased fiber roughness and enhanced porosity; however, the fiber mats displayed high water droplet-adhesion. The $SiO_2$–incorporated fibrous mats were then treated with stearic acid at an activation temperature of 80 °C. This treatment caused fiber surface plasticization, creating a tertiary hierarchical roughness owing to the interaction of PHBV chains with the polar carboxyl groups of the stearic acid. Scanning electron microscopy was used to assess the influence of the electrospinning process parameters and the incorporation of nanoparticles on surface morphology of the fibers; energy dispersive X-ray spectroscopy confirmed the presence of $SiO_2$ nanoparticles. Fourier transform infrared spectroscopy was performed to study the incorporation of $SiO_2$ and the interaction of stearic acid with PHBV at various concentrations. The chemical interaction between stearic acid and PHBV was confirmed, while $SiO_2$ nanoparticles were successfully incorporated into the PHBV fibers at concentrations up to 4.5% by weight. The incorporation of nanoparticles and plasticization altered the thermal properties of PHBV and a decrease in crystalline fraction was observed. The stearic acid modified bilayers produced from the micro-nano-fibrous composites showed very low water droplet sticking, a roll off angle of approximately 4° and a high static contact angle of approximately 155° were achieved.

**Keywords:** Electrospinning, Superhydrophobicity, PHBV/$SiO_2$ composites, Biopolymers, Nanoparticles, Fiber surface modifications

*Correspondence: saad.rabbani1@uqac.ca; saad.rabbani1989@gmail.com
Department of Applied Sciences, University of Quebec in Chicoutimi (UQAC), 555 boul. de l'Université, Chicoutimi, Quebec G7H 2B1, Canada

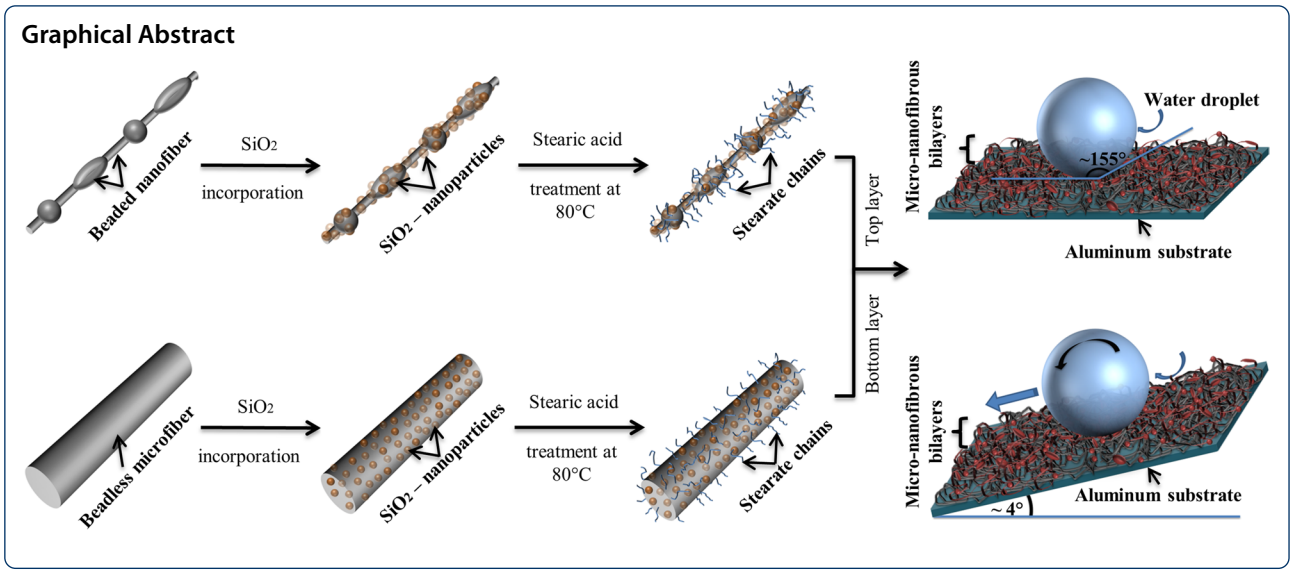


## Introduction

The behavior of a water droplet upon interaction with a surface reflects the material properties of that surface, such as chemistry, texture/morphology and surface energy. In general, the wetting state, static water contact angle (WCA), and dynamic roll-off of a water droplet on a surface are the primary indicators of the hydrophilic, hydrophobic or superhydrophobic nature of a material. As a rule, surfaces having a WCA $\geq 150°$ and roll-off angles $\leq 10°$ are considered to be superhydrophobic surfaces [1]. Bioinspired superhydrophobic surfaces with hierarchical morphologies have received much attention over the past three decades having various applications in material science/engineering [2–9].

Polyhydroxyalkoanates (PHAs) are a broad class of biopolymers produced by the fermentation process of microorganisms and bacteria in the presence of a carbon – rich source and limiting nutrients [10]. Different types of PHAs have been studied; each PHA is classified according to the length of its side chain and molecular weight. Among several studied strains, the copolymer of polyhydroxybutyrate (PHB) and polyhydroxyvalerate (PHV) or poly(3-hydroxybutarate-*co*-3-hydroxyvalerate) labeled PHBV is the most widely studied biocompatible microbial polyester. PHB is the most viable industrial type of PHA, as it has very similar physical properties to conventional plastics, e.g., isotactic polypropylene [11]. PHV is a variant of PHB having an ethyl group instead of a methyl group and is usually copolymerized with PHB in small concentrations to enhance flexibility, improve mechanical properties and delay the biodegradation time of PHBV [12].

The incorporation of fillers into the PHBV fiber matrix has been extensively explored to induce extrinsic properties. These studies include PHBV electrospun with Zinc oxide (ZnO) for antibacterial properties [13, 14]; PHBV incorporated with carbon nanotubes (CNTs) for superior mechanical stability and enhanced water repellence [15–17]; graphene and graphite nanosheets to induce electrical and electromagnetic properties [18, 19]; PHBV/Titanium dioxide ($TiO_2$) composites for improved physio-chemical properties and cytocompatibility [20]; and PHBV/polyethylene oxide (PEO) fibrous scaffolds [21] having superior mechanical stability for tissue engineering. $SiO_2$ nanoparticles (NPs) are extensively used as functional fillers in various applications particularly hydrophobicity owing to superior thermal and chemical stability along with their ability to be functionalized due to the presence of silanol groups [22]. Additionally, $SiO_2$–NPs are cheap and readily available and are not hazardous to environment compared to fluorinated additives. Several works on the use $SiO_2$–NPs as fillers in organic polymer matrices have been carried out, e.g. Sriram et al. [23] created porous superhydrophobic polymethylmethacrylate (PMMA)/$SiO_2$ coated filter papers for oil–water separation, Qing et al. [24] created polyvinylacetate (PVA)/$SiO_2$ nanofibrous membranes with superhydrophilic/superoleophobic properties, Ji et al. [25] used electrospinning to create ultrafine polyacrylonitrile (PAN)/$SiO_2$ composite nanofibers while Newsome et al. [26] electrospun polyvinylpyrrolidone (PVP)/$SiO_2$ composite fibers with high NP concentration and varying morphologies. On the other hand, the hydrophobicity of polyurethane (PU) was enhanced using $SiO_2$–NPs owing to phase separation and particles aggregation on the surface in a work by Seyfi et al. [27]. Meanwhile, $SiO_2$–incorporated PHBV composites have been produced via melt-blending [28], solution casting [29], hot-press

molding [30], and dispersion in a twin-screw extruder [31] as means to manipulate the crystallization and thermo-mechanical properties of the PHBV biopolymer, and although PHBV/$SiO_2$ electrospun mats have been recently studied for antibacterial properties [32], there are currently no reports mentioning the electrospinning of $SiO_2$ incorporated PHBV fibers to create superhydrophobic surfaces.

The use of long-chain fatty acids as plasticizers for PHBV to enhance ductility and induce flexibility have been discussed by Moser et al. [33]. They investigated the effects of chain length, blend concentration, and the degree of saturation of different fatty acids on the mechanical properties of PHBV. The oxygen-containing polar functional group in stearic acid (SA) appears to interact with PHBV, whereas the presence of any long side chains or unsaturated bonds in other fatty acids can hinder this interaction. Requena et al. [34] studied the effect of different plasticizers on the thermal properties and degree of crystallinity of PHBV films. When plasticizers were added to rigid polymers, they interacted with the polymeric backbone to form intramolecular bridges that reduces the mechanical stiffness [35] and alters the physical properties, e.g., roughness, by creating a "free volume" [34, 36]. Jost et al. examined the impact of different plasticizers like propylene glycol, glycerol, triethyl citrate, castor oil, epoxidized soybean oil and polyethylene glycol on crystallinity, ductility and tensile properties of PHBV blends [36]. They argued that substances having polar functional groups could be used as surfactants for plasticization and tend to interact with PHBV. They also discussed that the presence of side chains and unsaturated bonds in certain plasticizers may hinder these interactions, meanwhile low molecular-weight fatty acid compounds may not have sufficiently strong interactions. Relying on these previous studies, saturated linear-chain SA was considered as being an ideal fatty acid for modifying the surface of PHBV fibers.

Electrospinning is a fast and simple technique for producing continuous fibers of various sizes and morphologies. The basis of electrospinning is the elongation of an electrified droplet of a polymer solution extruded through a capillary by surface tension [37]. Different types of fibers having a high surface area and low surface energy from a few nanometers to several micrometers in thickness can be created. A variety of polymers, copolymers, and composites have been electrospun in solution for a range of applications [38–41].

In this study, we have adopted a fast and cheap method to synthesize superhydrophobic PHBV/$SiO_2$ composite fibers from an intrinsically hydrophilic PHBV strain (Supplementary S1a). The use of hydrophobic $SiO_2$ in electrospinning solution eliminates the need for any surface texturing processes and enables high fiber surface porosity. Meanwhile, surface plasticization using SA treatment influences the physical and thermal properties of the composite. Electrospun PHBV has been used in the food packaging industry, biomedical implants, fibrous scaffolds for tissue engineering, drug delivery systems [42–44], while superhydrophobic surfaces created from biopolymers find potential applications which require cytocompatibility [45–48], for oil–water separation, in filtration systems [49], etc. The novelty of this work revolves around the combination of the use of hydrophobic $SiO_2$–NPs in electrospun PHBV fibers and a simple post treatment using SA to create superhydrophobic composites. Biopolymers are gradually replacing conventional plastics in numerous applications, and we aim to use our developed superhydrophobic fibrous surfaces for these innovative applications that require enhanced water repellence.

## Experimental setup

### Materials

P(HB-*co*-HV) with 5% PHV concentration was kindly supplied as samples from Be-Up Biotechnology Inc., Quebec, Canada. PDMS-treated fumed – $SiO_2$ nanoparticles (AEROSIL R202), were supplied by EVONIK, Germany. High purity (> 95%, FCC, FG) stearic acid and 99% pure chloroform having 0.5%—1.0% ethanol as a stabilizer were purchased from Sigma Aldrich. Pure acetone was purchased from Fisher Chemicals, USA.

### Sample preparation

In this study, single-needle laboratory-scale electrospinning equipment was used to produce high-quality PHBV fibrous mats. The electrospinning parameters were carefully controlled to obtain the optimal fiber morphologies (Supplementary S1b). The needle that acts as a capillary, having an inner diameter of 400 µm (gauge no. 22) was connected to a DC-power supply unit, which could generate a voltage up to 40 kV. A 20 kV voltage and a fixed collector distance of 10 cm were determined to be sufficient for obtaining consistent fiber morphologies and successful solvent evaporation respectively. A mass flow rate of 1 mL/h was used to minimize the formation of fiber defects using a 5 mL syringe with the polymer solution as an extruder with fiber deposition directed toward a grounded steel collector. PHBV solutions of different concentrations (from 4 wt.% to 21 wt.%) in chloroform as a solvent were prepared; the choice of chloroform was made in accordance to the literature [50, 51].

After optimizing the electrospinning parameters for pure PHBV fibers, PDMS-treated fumed-$SiO_2$–NPs were added to the electrospinning solutions to produce PHBV/$SiO_2$ composite fibers; the NPs induced primary

roughness and reduced wetting. Relative concentrations of 1 wt.% to 6 wt.% $SiO_2$–NPs were added to test the influence of various concentrations of functionalized NPs on wetting time delay. Relying on our observations of solution spinnability and the resulting fiber morphology, optimal $SiO_2$–NP concentrations of 3 wt.% and 1.7 wt.% were selected for the beadless microfibers and beaded nanofibers, respectively.

In the second step, the surface of the electrospun PHBV/$SiO_2$ composite fibrous mats were modified by treating them with saturated linear-chain SA, thereby creating tertiary roughness on the fiber surface (Supplementary S1c). Surface modification using SA can readily improve the ductility and flexibility of PHBV/$SiO_2$ composites upon plasticization [33–36], and it can also improve the hydrophobicity of an otherwise hydrophilic biopolymer owing to an increased roughness and the presence of low surface energy materials [52]. Bilayers of beadless microfibers and beaded nanofibers produced from the two different optimized PHBV/$SiO_2$ composite fibers were modified in a SA/acetone solution at an elevated temperature. Different authors have discussed the high temperature activation of SA near and above its melting temperature of 69.5 °C [53, 54]. Therefore, a reaction temperature of 80 °C was used to modify the bilayers using various concentrations of SA, from 1 wt.% to 12 wt.%, dissolved in acetone solvent. The SA/acetone solutions were prepared using a heated magnetic stirrer, and the composite samples were immersed into this solution for 1 to 3 min. SA exhibited a good dissolution in acetone [52] whereas the PHBV/$SiO_2$ composites remained insoluble in acetone even at 80 °C. After their modification, the samples were dried at 90 °C for 1 h in air to evaporate the solvent.

## Analytical characterizations

### Optical/Scanning electron microscopy

Optical microscopy (Nikon Eclipse E600 Pol optical microscopy) was carried out on the fibrous mats at 200× magnification to verify fiber quality after each deposition. The morphology of the electrospun PHBV fibers was then observed using scanning electron microscopy (SEM, JSM-6480LV, JEOL). The samples were gold-coated prior to SEM analysis. Pure PHBV fibers, PHBV/$SiO_2$ composite fibers and SA modified mats were observed to compare changes in surface morphology at each step of the fiber surface modification process. Energy-dispersive X-ray spectroscopy (EDX) utilizes characteristic X-rays from backscattered electrons. Addition of a secondary detector can enable us to identify elemental species and EDX was used to confirm the presence of $SiO_2$–NPs in the PHBV fiber composite.

### Fourier transform infrared spectroscopy

Fourier transform infrared spectroscopy (FTIR) was used to analyse the effect of different concentrations of SA for PHBV surface modification. A scan range of 650 $cm^{-1}$ to 4000 $cm^{-1}$ was performed using an Agilent Cary 630 spectrophotometer by ATR method with a 2 $cm^{-1}$ resolution.

### Differential scanning calorimetry

The effect of surface modifications on thermal properties was evaluated using differential scanning calorimetry (DSC), specifically, the phase change thermodynamics of the PHBV/$SiO_2$ composite upon modification with SA. "Discovery model TA-DSC 25" was used to determine melting temperature ($T_m$) and melting enthalpy ($\Delta H_m$) of the synthesized composite fiber mats. The change in the degree of crystallinity was calculated using Eq. 1 (for pure PHBV) [55] and Eq. 2 (For PHBV/$SiO_2$ composites) [30].

$$X_c(\%) = \frac{\Delta H_m}{\Delta H_m^o} \times 100 \tag{1}$$

where $X_c$ is the degree of crystallinity, $\Delta H_m$ is the measured melting enthalpy of PHBV. The theoretical enthalpy of PHBV ($\Delta H_m^o$) was taken to be 109 J/g [14].

$$X_c(\%) = \frac{\Delta H_m}{(1 - W_f)\Delta H_m^o} \times 100 \tag{2}$$

$W_f$ is the weight fraction of inorganic $SiO_2$ incorporated into the fiber composites. PHBV powders, as-received SA powders, pure PHBV fibers, PHBV/$SiO_2$ composite fibers, and SA modified PHBV fibers were all investigated. Samples were placed into a sealed aluminum pan under a 50 mL/min nitrogen flow. The heating cycles were carried out on each sample from 20 to 200 °C at a rate of 10 °C/min.

### Contact angle measurements

Static water contact angles (WCAs) and wetting time analysis were performed using a drop shape analyzer DSA100 (Kruss GmBH, Germany). The WCA measurements were done using the sessile droplet method with a 4 µL droplet of distilled water; averages of five measurements for each sample were conducted (Supplementary S1d). The dynamic roll-off angle was determined as the angle of an inclined plane required to cause a water droplet to roll off from a surface.

## Results and discussions

### Surface morphology

Applying the electrospinning parameters discussed in the Sample preparation section, the PHBV concentrations

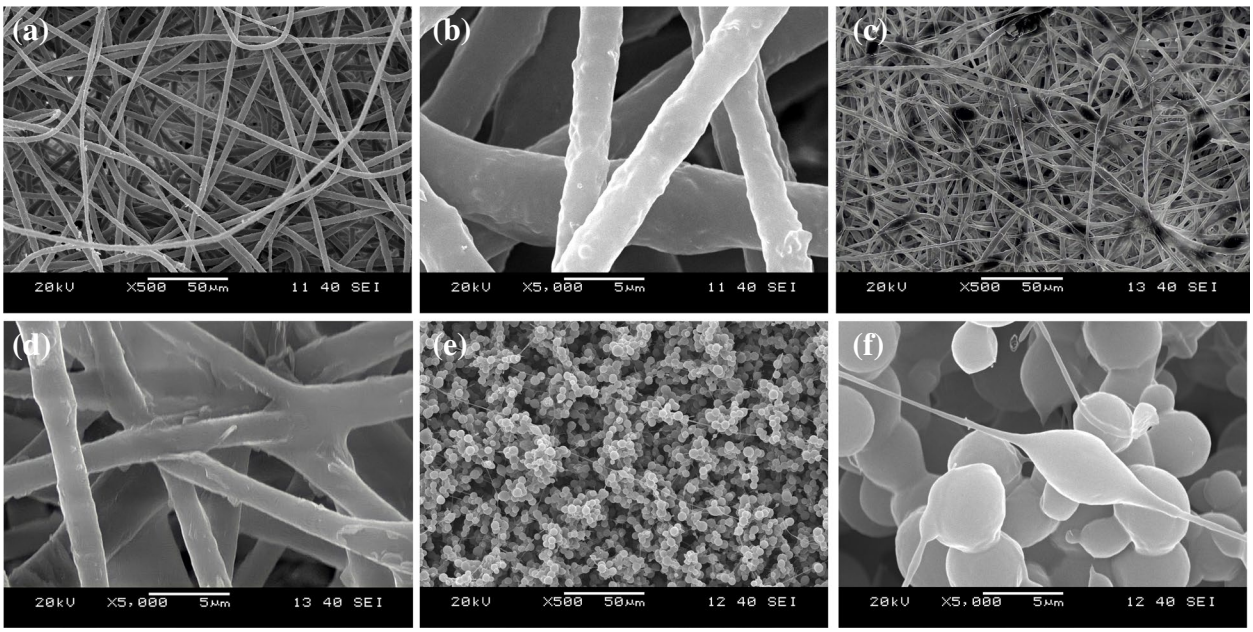


**Fig. 1** SEM images of pure PHBV fibers at two magnifications (500x, 5000x). **a**, **b** Beadless microfibers from a 21 wt.% PHBV solution; **c**, **d** beads on microfibers from a 12 wt.% PHBV solution; **e**, **f** beaded nanofibers produced from a 4 wt.% PHBV solution

were decreased from 21 wt.% to 4 wt.%; therefore, solution concentration was the only variable parameter to obtain a beaded morphology. As expected, with the decrease in PHBV concentration, the appearance of a beaded morphology was observed along with a decreasing fiber thickness.

SEM images captured at different magnifications showed that fibers synthesized from 21 wt.% pure PHBV solutions (Fig. 1a, b) had no beads and were characterized by a smooth continuous morphology. Fiber thickness, calculated from 22 measurements, averaged $3.94 \pm 0.42$ µm (Supplementary S2a). By decreasing the solution concentration to 12 wt.%, the appearance of a bead-on-fiber morphology was observed (Fig. 1c); some intertwining at higher magnification (Fig. 1d) was also noticed along with a decrease in fiber thickness to an average of $2.55 \pm 0.32$ µm, as determined from 23 measurements (Supplementary S2b).

A further reduction in the solution concentration to 4 wt.% PHBV produced a "pop-corn like" morphology, which has been reported previously for very dilute concentrations [43]. The dependence of beaded morphology on the hydrophobicity of the pure PHBV fibrous surfaces has been discussed by other researchers. Zuo et al. [43] electrospun very low concentration solutions and reported WCAs of ~ 110° using 4 wt.% PHBV solution in chloroform. In contrast, Moon et al. [56] produced beadless PHBV fiber mats using 28 wt.% and observed an initial WCA of ~ 128°; they observed a high density of beads on microfibers at their lowest concentration of 16 wt.%, resulting in a WCA of ~ 123°. In this study, a beaded morphology along with the presence of nanoscale fibers was obtained (Fig. 1e, f) using a 4 wt.% PHBV solution. The average diameter of the beads taken from 25 measurements was found to be $4.25 \pm 0.93$ µm (Supplementary S2c). The surfaces of both the fibers and beads however, lack porosity (Fig. 1b, d and f), in both beadless microfibers and beaded nanofibers, thereby indicating an absence of a hierarchical roughness.

PDMS-treated $SiO_2$–NPs were incorporated into 12 wt.% and 4 wt.% PHBV solutions and, using SEM imaging, a change in fiber surface morphology was observed (Fig. 2). For these composite fibers, a 12 wt.% PHBV concentration for the microfibers was used because a further increase in solution viscosity in the presence of $SiO_2$–NPs would clog the capillary due to drag resistance [57]. Meanwhile, at concentrations less than 4 wt.% PHBV, there was insufficient time for the solvent to evaporate when using the predetermined electrospinning parameters. As anticipated, the incorporation of NPs created surface roughness in each case. This roughness was, however, more pronounced in the beaded nanofibers than the beadless microfibers. This is because a higher concentration of PHBV was extracted during electrospinning of 12 wt.% PHBV solutions in contrast to 4 wt.% PHBV solutions using the same feed rate of 1 mL/h in both cases. Therefore, the 12 wt.% electrospun microfibers obtained a greater coverage

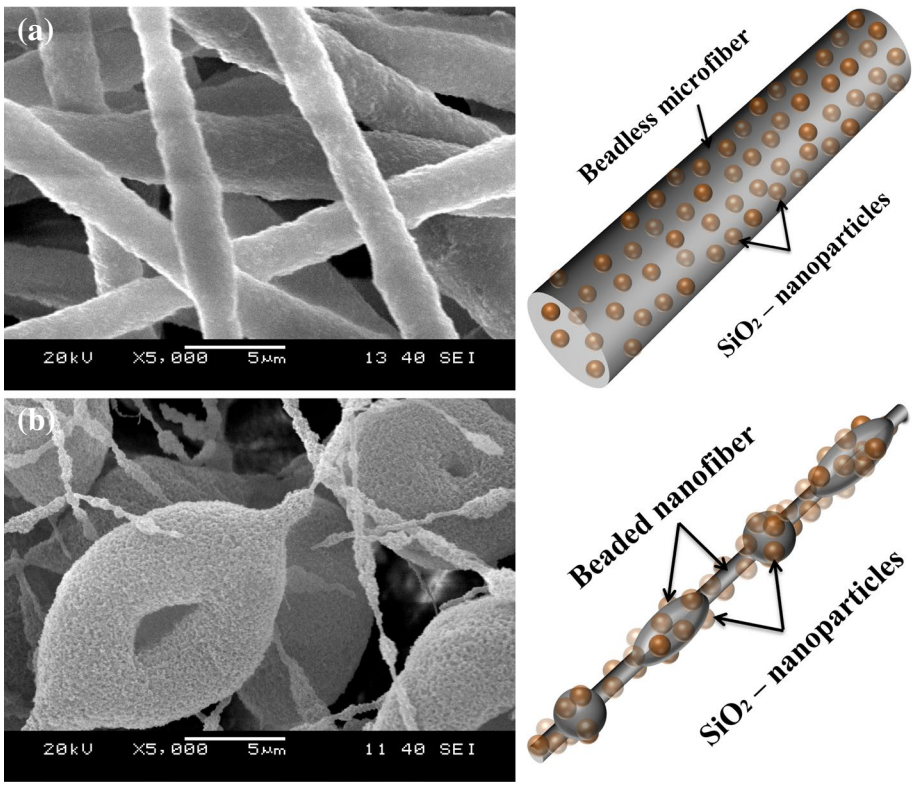


**Fig. 2** SEM images of $SiO_2$–incorporated PHBV fibers; **a** beadless microfibers from a 12 wt.% PHBV solution; **b** beaded nanofibers from a 4 wt.% PHBV solution; **c**, **d** schematics of each morphology

of NPs with the PHBV matrix (Fig. 2a, c) compared to much superior roughness of beaded nanofibers from 4 wt.% solutions (Fig. 2b, d).

Various authors have discussed the effect of beaded fiber morphology on the mechanical properties of fibers produced from low viscosity electrospinning solutions [58–60]. Hence, increasing roughness may result in reduced mechanical strength, abrasion resistance and ductility due to higher defect density [61]. Therefore bilayers of fibrous mats (at 12 wt.% and 4 wt.% PHBV solution concentrations) were produced to observe the synergic properties of higher fiber surface roughness and stable fibrous membranes. The bilayer composite mats were then observed under SEM (Fig. 3). At higher magnifications (Fig. 3b); with the focus on the top layer of beaded nanofibers, the beadless microfibers can be observed in the background as the bottom layer.

The effect of SA modification on PHBV/$SiO_2$ fiber surfaces can only be visualized clearly for microfiber composites (Fig. 4). The SEM images show high surface roughness upon plasticization by SA and the creation of "free volume" as anticipated, inducing hierarchical roughness. It was assumed that the same influence of SA modification occurred in the case of beaded nanofiber composites; however, this change could not be observed under SEM due to the presence of the high density of defects and relatively higher roughness induced in beaded nanofibers after incorporating $SiO_2$–NPs.

The presence of $SiO_2$–NPs in the PHBV fiber matrix was confirmed using EDX. Figure 5 presents the point scans taken on fibers from pure PHBV, PHBV/$SiO_2$ composites and SA modified composites. Table 1 compares the relative change in the atomic percentages of carbon, oxygen and silicon for unmodified and SA modified PHBV/$SiO_2$ composites relative to pure PHBV fibers.

EDX spectra confirm the presence of a high concentration of silicon at 1.74 keV (Fig. 5b, c) compared to pure PHBV fibers (Fig. 5a). As the point scans were ran on the individual fibers of each sample, it was confirmed that a successful incorporation of $SiO_2$–NPs was carried out within the PHBV fiber matrix during electrospinning. Moreover, when the same sample of PHBV/$SiO_2$ composite (example in Fig. 5b) was surface modified with SA, the relative ratio of carbon to silicon was increased (Fig. 5c). The surface modification with SA inevitably alters the overall ratio of carbon, oxygen, and silicon in the composites.

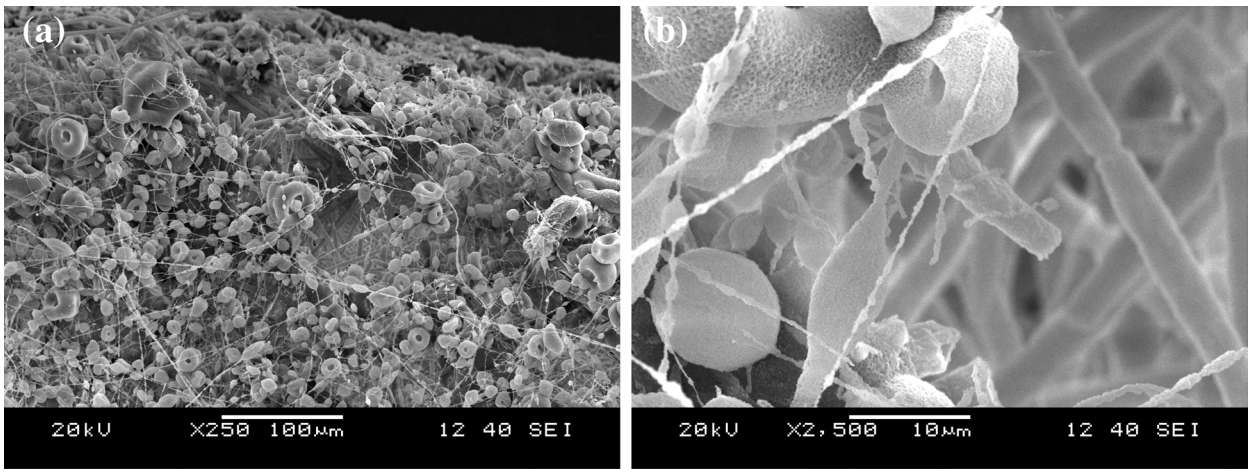


**Fig. 3** SEM images of bilayers of $SiO_2$ incorporated beadless microfibers (3 wt.% $SiO_2$) and beaded nanofibers (1.7 wt.% $SiO_2$) at different magnifications showing micro-nano-fibers within the same sample

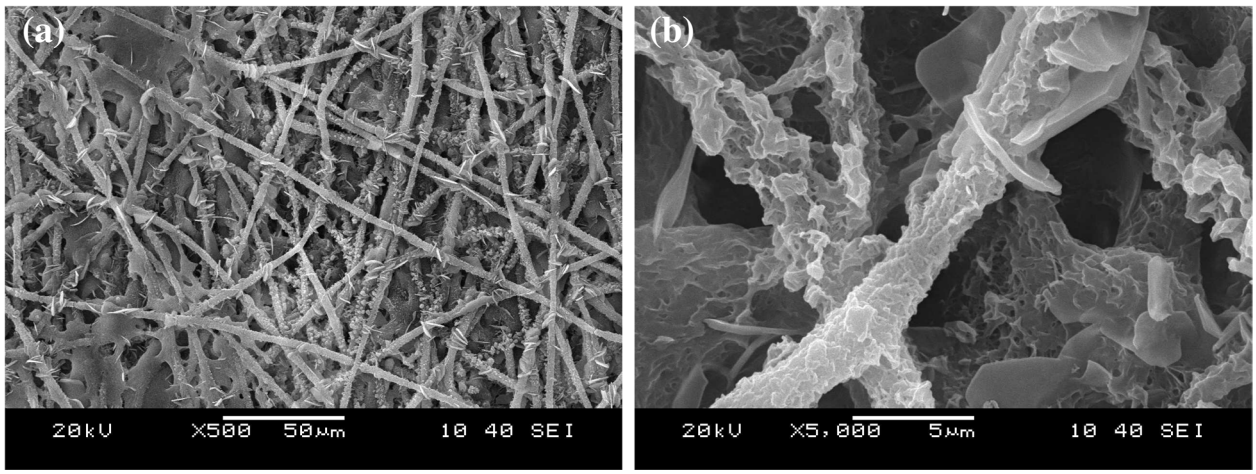


**Fig. 4** SEM images of PHBV microfibers with 3wt.% $SiO_2$-incorporated PHBV modified with a 5 wt.% SA-solution

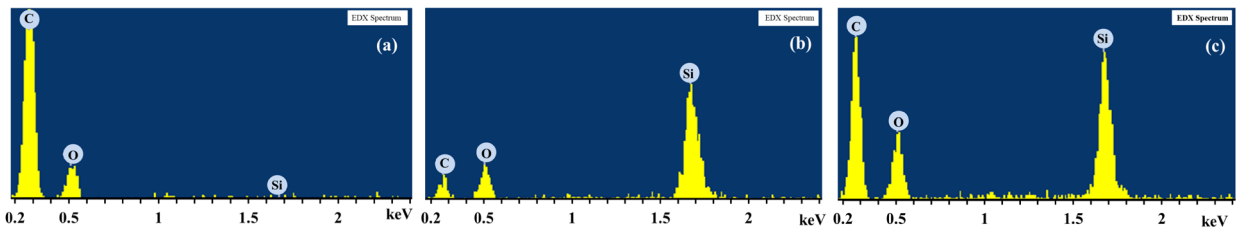


**Fig. 5** EDX spectra of **a** pure PHBV fibers, **b** PHBV/$SiO_2$ composite fibers, and **c** SA modified composites

## Thermal analysis

DSC was used to study the change in melting temperature and melting enthalpy of PHBV following the incorporation of $SiO_2$–NPs and the surface modification by SA. Solutions of varying concentrations of SA in acetone (e.g., 2 wt.%, 5 wt.% and 12 wt.%) were used

**Table 1** Relative change in carbon and oxygen content following $SiO_2$ incorporation and SA modification

| Sample | Pure PHBV | PHBV/$SiO_2$ (unmodified) | PHBV/$SiO_2$ (SA modified) |
|---|---|---|---|
| %Carbon | 73.1 ± 1.64 | 52.5 ± 2.25 | 66.7 ± 3.02 |
| %Oxygen | 26.9 ± 1.63 | 40.2 ± 3.15 | 28.5 ± 4.9 |
| %Silicon | 0.017 ± 0.02 | 7.28 ± 0.96 | 4.8 ± 2.1 |

to modify the surface of 12 wt.% PHBV fibers in each sample to optimize the extent of plasticization of PHBV fibers and minimize residual SA in the resultant fibrous mats. The thermal properties of the SA modified PHBV fibers were compared with those of pure PHBV (Fig. 6). The effects of $SiO_2$–NPs and SA modification on melting temperature and enthalpy are summarized in Table 2.

When melting at a constant rate, pure PHBV showed a high degree of crystallinity (Sample 1 in Table 2). Adding 3 wt.% $SiO_2$ (Sample 2) into the electrospinning solution did not affect the melting temperature markedly; however, the melting enthalpy and therefore the degree of crystallinity reduced noticeably. Several reasons could account for the decrease in enthalpy with the addition of $SiO_2$–NPs. First, the difference in the respective specific heats of NPs and the PHBV matrix could account for the overall decrease in thermal absorbance as NP concentration increased; the result is an overall decrease in the latent heat of fusion of the PHBV/$SiO_2$ composite. Second, the thermal conductivity of NPs can influence the heat transfer characteristics of the composites, thereby reducing the overall enthalpy of the composites. Finally, the high surface area and the possibility of agglomeration could cause heterogeneity in nanoparticle distribution and provoke an instability that decreases melting enthalpy. That said, it is also evident that increasing the SA concentration decreases both the melting temperature and melting enthalpy of the PHBV fibers (Samples 3 and 4), which indicates a chemical change to the PHBV [36, 62]. The interaction of the polar groups of SA molecules with the PHBV fibrous mats presumably affects the intramolecular structures of the PHBV chains. This altering of the PHBV structure decreases the degree of crystallinity which can be predicted from the lowering of melting enthalpy after surface modification of PHBV fibers. The change in intramolecular forces in PHBV chains upon plasticization with SA decreases crystallinity, as also shown in previous literature [34].

In the final sample (Sample 5) the synergic effects of $SiO_2$–NPs and SA modification on the thermal properties of PHBV are evident. $SiO_2$–NPs are assumed to decrease melting enthalpy, whereas the SA modification decreases the melting temperature in the same sample. Data of the first melting enthalpy supports this hypothesis, as the incorporation of $SiO_2$–NPs sharply decreased $\Delta H_m$ (Sample 2) in contrast to the pure PHBV (Sample 1), whereas relatively higher $\Delta H_m$ was observed in the SA modified PHBV fibers (Sample 3 and 4). The combination of $SiO_2$ incorporation with 5 wt.% SA modification in sample 5 therefore produced the lowest observed crystallinity values. Hence, it can be anticipated that incorporation of NPs into the PHBV matrix, combined with SA plasticization, not only induces roughness in the fibrous membranes but also reduces PHBV stiffness caused by a reduced crystalline fraction.

### FTIR analysis

FTIR analyses of PHBV fibrous mats modified with different concentrations of SA in an acetone solution are shown in Fig. 7a; these samples are compared to pure PBHV and pure SA. Pure PHBV produces a strong signal at 1720 $cm^{-1}$ corresponding to the C=O stretching bond, which is characteristic of ester groups. Secondly, two weak signals at 2930 $cm^{-1}$ and 2974 $cm^{-1}$ represent aliphatic alkyls in the functional group region originating from the C-H stretching bonds of ethyl and methyl, respectively. For pure SA, there is an absence of absorption bands at 3009 $cm^{-1}$ and 1654 $cm^{-1}$, which normally correspond to unsaturated C=C deformation vibrations and stretching vibrations respectively [33]. This absence of C=C verifies that the SA used in this work was a saturated linear-chain fatty acid which was a prerequisite for successful molecular interaction at the polar carboxylic

**Table 2** Thermal analysis results obtained from DSC measurements of various samples

| # | Sample | Melting temperature ($T_m$) °C | Melting enthalpy | %Crystallinity |
|---|---|---|---|---|
| 1 | Pure PHBV | 158.55 | 70.14 | 64.3 |
| 2 | PHBV fibers (3 wt.% $SiO_2$) | 157.79 | 39.03 | 36.9 |
| 3 | PHBV 2 wt.% SA modified | 155.43 | 52.67 | 48.3 |
| 4 | PHBV 12 wt.% SA modified | 153.99 | 44.7 | 41 |
| 5 | PHBV with 3 wt.% $SiO_2$–NPs (5 wt.% SA modified) | 153.8 | 31.2 | 29.5 |
| 6 | Pure SA | 69.5 | 221.08 | - |

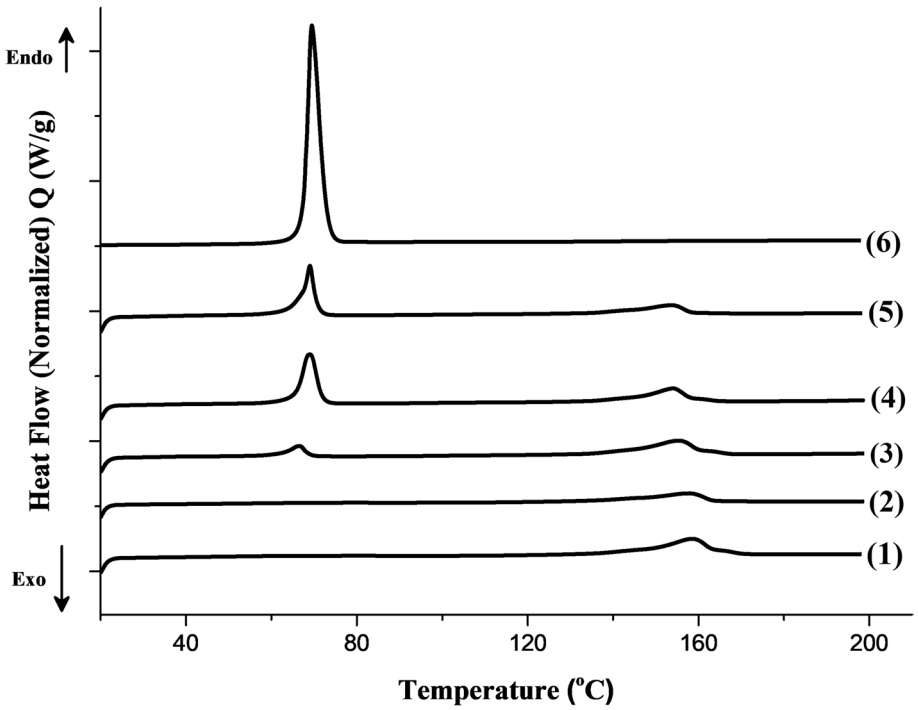


**Fig. 6** DSC thermograms of the first heating cycles of (1) pure PHBV samples, (2) PHBV/$SiO_2$ composite fibers (unmodifed), (3) PHBV fibers with 2 wt.% SA modification, (4) PHBV fibers with 12 wt.% SA modification, (5) PHBV/$SiO_2$ composite with 5 wt.% SA modification and (6) pure SA

end with PHBV, as discussed in the literature [35, 36]. Furthermore, the C=O stretching peak for pure SA, corresponding to a signal at 1696 $cm^{-1}$ and having a relatively weaker transmittance represents conjugate acids.

FTIR was also used to characterize PHBV/$SiO_2$ composite fibers with increasing $SiO_2$–NPs concentration from 1 wt.% to 4.5 wt.% relative to a 12 wt.% PHBV/chloroform solution. The spectra were compared to those of pure PHBV fibers and pure $SiO_2$–NPs (Fig. 7b). The $SiO_2$–NPs were incorporated into the PHBV fiber matrix and apparently did not influence the chemical structure of the PHBV matrix. As the concentration of NPs was increased (even as high as 4.5 wt.%), no characteristic absorption peaks from the $SiO_2$ interaction with PHBV were observed, thus indicating physical incorporation into the composite. Finally, the FTIR spectra of the synergic effect of $SiO_2$–NPs and SA modified fibers is shown in Fig. 7c. Evidently, except for the characteristic stretching peak of $SiO_2$ at 1083 $cm^{-1}$ in the fingerprint region, no other interaction peaks are observed prior to SA treatment which confirms the above hypothesis that the inorganic $SiO_2$ is physically incorporated in PHBV fibers. On the other hand, as concentrations of SA in PHBV increased, a gradual shift in the characteristic signal of PHBV at 1720 $cm^{-1}$ to a lower wavenumber was observed (Fig. 7b). This shift indicated an interaction of the PHBV chains with the oxygen–containing polar group of SA. Furthermore, no visible change in the FTIR spectra of the PHBV fibers treated with 1 wt.% SA solution was observed compared with those of the pure PHBV fibers. This absence of a change could be due to a very low concentration of SA molecules, thereby decreasing the probability of homogeneous molecular interactions of SA with PHBV in the sample. However, as SA concentration increased, the C-H stretching bonds at 2915 $cm^{-1}$ and 2848 $cm^{-1}$ appeared; these are characteristic absorption peaks of long–chain alkanes. With a gradual increase in SA concentrations, the former peak of SA appeared to overlap with the latter peak of pure PHBV in the functional group region, which at first glance indicates an interaction between the C-H alkyl groups. However, given that an interaction of PHBV and SA is more probable at the oxygen-containing polar groups, the overlapping of saturated alkane peaks for the both components can be considered an artifact of the final product, having different methyl, ethyl and, stearate groups.

### Wettability behavior

WCAs of the fibrous surfaces were compared with casted films from the same solutions. Pure PHBV fibrous mats showed complete wetting with an almost instantaneous droplet collapse for the 21 wt.% and 12 wt.% PHBV

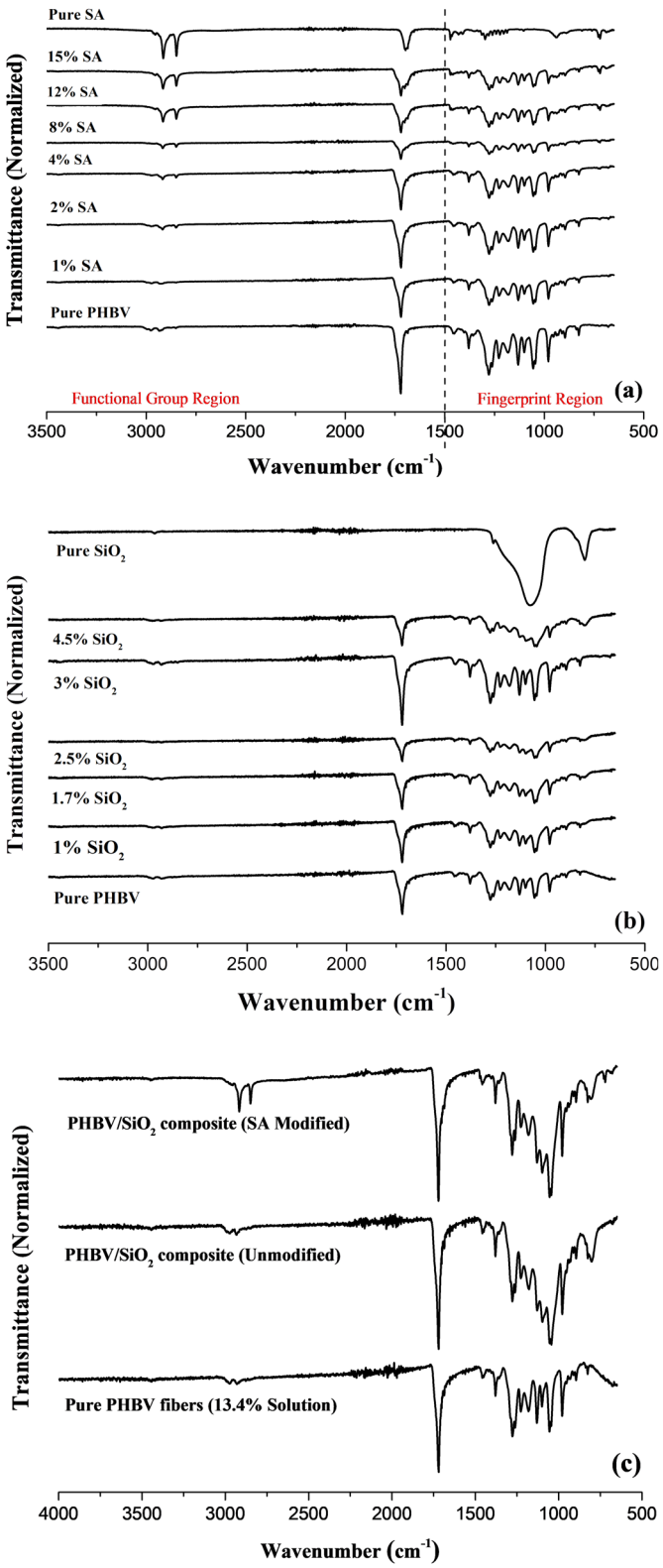


**Fig. 7** FTIR of **a** SA modification on PHBV fibers; **b** PHBV/$SiO_2$ composite fibers and **c** synergic effect of $SiO_2$ incorporation and SA modification on PHBV fibers

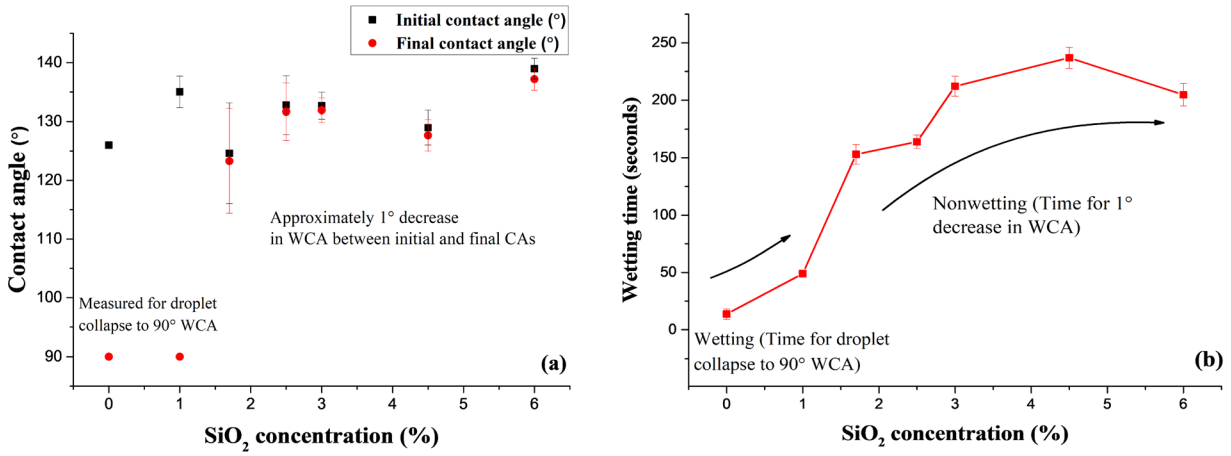


**Fig. 8** **a** Variation in the initial WCAs of PHBV/$SiO_2$ composite fibrous mats with increasing concentrations of $SiO_2$–NPs. **b** Evaluation of droplet collapse time of PHBV/$SiO_2$ composite fibrous mats as a function of $SiO_2$–NP concentration

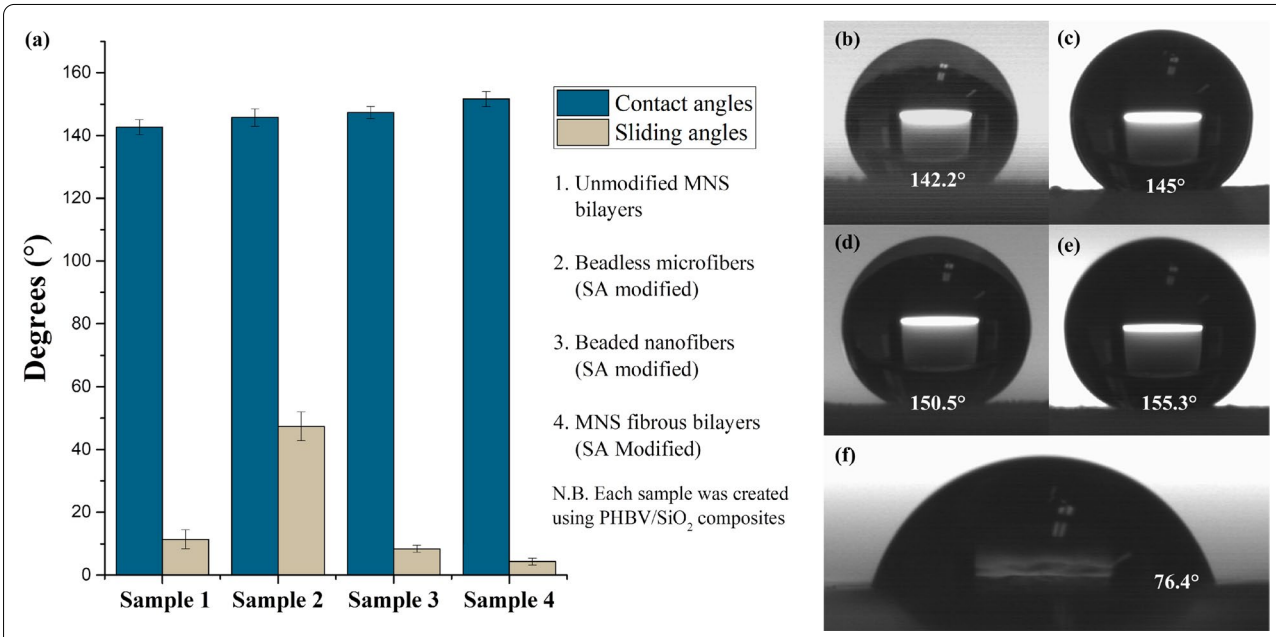


**Fig. 9** **a** Comparison of the WCAs and sliding angle of a 4 µL water droplet for four different sample designs; **b** micro-nanofibrous (MNS) bilayers before SA treatment; **c** SA modified beadless microfibers; **d** SA modified beaded nanofibers **e** SA modified MNS bilayers **f** PHBV/$SiO_2$ film cast on a glass slide

solutions (Supplementary S3a). Decreasing the concentration of PHBV increases the droplet collapse time due to the appearance of the rough beaded nanofiber morphology [43, 56]. However, even at low concentrations, pure PHBV mats showed a predominantly wetting behavior and very low static contact angles were observed after droplet collapse, the reason for this is the absence of a secondary hierarchical roughness (Fig. 1f). The film cast from solution in each case showed WCAs in the range of 75° to 80° (Fig. 9f), values that agree reasonably well with those in the literature [43].

Incorporation of $SiO_2$–NPs changes the wetting state to a Wenzel non-wetting state caused by the partial encapsulation of the NPs within the fiber morphology, which creates the required fiber surface roughness (Supplementary S3b). Different concentrations of $SiO_2$–NPs (from 1 wt.%

to 6 wt.%) were added to 12 wt.% PHBV solutions prior to electrospinning. The obtained initial WCAs for different $SiO_2$ concentration were in the range of 125° to 141° (Fig. 8a). The change in wettability of the fibrous mats as a function of $SiO_2$–NPs increased the droplet collapse time with increasing $SiO_2$–NPs concentration (Fig. 8b). As mentioned above, water droplets collapsed rapidly for the pure PHBV fibers (without $SiO_2$–NPs) and relatively slower at 1 wt.% $SiO_2$ because of the resistance caused by hydrophobic NPs and hydrophilic PHBV matrix. The average time required for a droplet to collapse from its initial WCA down to 90° was 13.6 ± 4.5 s for pure PHBV fibers and 49 ± 2.2 s for 1 wt.% $SiO_2$ incorporated fibers. When the $SiO_2$ concentration increased to 1.7 wt.%, the wettability state changed to a non-wetting state, and the water droplet ceased to collapse. Now in all the cases with $SiO_2$ concentration higher than 1.7 wt.%, the time required for the WCA to decrease by approximately 1° was determined using a video recorder (Fig. 8b). The highest initial WCAs of 132.8° ± 4.99° and 132.7° ± 2.28° were obtained at the respective $SiO_2$ concentration of 2.5 wt.% and 3 wt.%. Negligible changes in WCAs were observed over an extended period with only a 1° decrease after 164 ± 5.92 s and 212 ± 8.79 s, respectively (Fig. 8b). Higher $SiO_2$–NP concentrations of 4.5 wt.% and 6 wt.% were discarded because of irregular trends probably caused by the heterogeneity/agglomeration of NPs within the fibers and the difficulty in electrospinning as excessive NPs would clog in the capillary. From these observations, it was concluded that the optimal static WCAs and delayed wettability for microfiber composites can be obtained using a 12 wt.% PHBV solution with a 3 wt.% concentration of $SiO_2$–NPs. On the other hand, for beaded nanofiber composites obtained from a 4 wt.% PHBV solution, a concentration of 1.7 wt.% $SiO_2$–NPs was considered optimal. Although the wetting state changed to a non-wetting state with the incorporation of PDMS-treated fumed $SiO_2$–NPs, the water droplet adhesion to the fibrous surface remained nonetheless high. This is attributed to the intrinsically hydrophilic nature of the PHBV matrix and the presence of a Wenzel state. The surface therefore showed no dynamic roll-off but rather a relatively high droplet sticking because of a lack of tertiary hierarchical roughness (Supplementary S3b).

Superhydrophobicity on such hydrophilic surfaces can be induced using several methods proposed in the literature [63]; for example, researchers have modified surfaces by plasma etching using fluorinated compounds to reduce the surface energy [56]. Nonetheless, the use of fluorinated compounds in a biopolymer is not ideal because of the associated environmental hazards. Complicated texturing processes are also not industrially viable. Hence, here the $SiO_2$-incorporated PHBV fibers were modified using a simple thermal activation reaction of PHBV with SA in an acetone solvent. The surface plasticization of PHBV, using long-chain fatty acids via the interaction of polar groups, produced the desired submicron roughness and also improved ductility [36]. The hierarchical structure markedly reduced water droplet adhesion, resulting in a dynamic roll-off via the transformation to a Cassie–Baxter state (Supplementary S3c).

The water repellency and sliding angles of four sample designs (Fig. 9)a were compared. In each case, $SiO_2$–NPs were incorporated using a concentration of 3 wt.% and 1.7 wt.% for the beadless microfibers and beaded nanofibers respectively. Samples 1, 3 & 4 (Fig. 9b, d & e) demonstrated much lower sliding angles owing to their higher surface roughness because of the presence of a beaded morphology in the top layer and high porosity fibers at the droplet-fiber interface in comparison to that of Sample 2 (Fig. 9c). The top layer in the case of micro-nano-fibrous (MNS) bilayer composites from 4 wt.% PHBV solution comprises a high density of beads and porosity compared to beadless microfiber composites from 12 wt.% PHBV solutions, which were previously used for droplet collapse measurements. Therefore, MNS composites facilitated a certain degree of dynamic roll-off even without surface modifications with SA (Sample 1). Sample 1 had, however, comparatively the smallest average static WCA of 142.7° ± 2.3°; therefore, surface modification with SA obviously improved the hydrophobicity of the bilayers, as illustrated by sample 4 showing an average WCA of 151.6° ± 2.1°. At the same time, the sliding angle in the case of MNS bilayers also decreased from 11.4° ± 3.02° to 4.3° ± 1.08° after treatment with SA, thereby indicating a direct influence on dynamic superhydrophobicity. Nonetheless, surface modified beadless microfiber composites showed improved static WCAs in the range of 145.8° ± 2.7°, relative to WCAs observed during the droplet collapse measurements; however, high droplet adhesion with sliding angles greater than 47° was observed in this case. This adhesion is reflected on the much lower surface roughness because of the higher degree of $SiO_2$–NPs encapsulation, the lower density of fiber porosities, more free space in between the thicker fibers enabling droplet interlocking and a hydrophilic PHBV matrix. Lastly, SA modified beaded nanofibers in Sample 3 (Fig. 9d) exhibited high WCAs of 147.3° ± 1.9° and a low droplet adhesion with sliding angles of 8.4° ± 1.1°. However, their use and applications are limited by the presence of a very high roughness and a "popcorn-like" morphology having a high defect density; these factors alter their mechanical properties [58–60]. It is therefore concluded that the surface modified MNS bilayer of the PHBV/$SiO_2$ composite is therefore an ideal design for superhydrophobic fibrous surfaces (Supplementary S1e & S3c), characterized by the highest contact angle of approximately 155.3° and roll-off angle of less than 4°.

## Conclusions

Superhydrophobic electrospun fibrous mats from PHBV/$SiO_2$ composites were produced using the intrinsically hydrophilic P(HB-*co*-HV) biopolymer. Solutions of pure PHBV in chloroform as solvent were prepared and electrospinning parameters were optimized to produce beadless microfibers and beaded nanofibers. The solution concentration of pure PHBV in a chloroform solvent played a critical role in producing the desired fiber morphology. PDMS-treated fumed $SiO_2$–NPs were incorporated into the electrospinning solution to modify the static wetting behavior of the fibrous mats owing to enhanced surface roughness. SEM was used to observe these changes in fiber morphology with the addition of NPs, and EDX analysis confirmed $SiO_2$ incorporation. The composite fiber mats were surface modified via interaction with SA to facilitate a dynamic roll-off by inducing a tertiary roughness upon the plasticization of PHBV/$SiO_2$ composites. The thermal analysis demonstrated that the incorporation of $SiO_2$–NPs and plasticization by SA decreased the crystallinity and altered the melting temperature of PHBV. FTIR analysis confirmed the interaction of the polar carboxyl groups of SA with the PHBV chains; however, the successful plasticization of PHBV/$SiO_2$ composites is limited to low SA concentrations. Superhydrophobic fibrous mats produced from bilayers of surface modified micro-nano-fibers demonstrated WCAs $\geq 155°$ and sliding angles $\leq 5°$ without the use of any fluorinated compounds or expensive texturing processes. Such biocompatible superhydrophobic surfaces offer several potential applications in, for example, biomedical technologies, drug delivery systems, cytocompatibility, water filtration, oil–water separation, and food packaging industries.

#### Abbreviations

DSA: Drop shape analyzer; DSC: Differential scanning calorimetry; EDX: Energy dispersive X-ray spectroscopy; FTIR: Fourier transform infrared spectroscopy; MNS: Micro-nano-fibrous structures; NPs: Nanoparticles; PAN: Polyacrylonitrile; PDMS: Polydimethylsiloxane; PEO: Polyethylene oxide; PHAs: Polyhydroxyalkoanates; PHB: Polyhydroxybutyrate; PHBV: Poly(3-hydroxybutarate-co-3-hydroxyvalerate); PHV: Polyhydroxyvalerate; PMMA: Polymethylmethacrylate; PU: Polyurethane; PVA: Polyvinylacetate; PVP: Polyvinylpyrrolidone; SA: Stearic acid; $SiO_2$: Silica; $TiO_2$: Titanium dioxide; $T_m$: Melting temperature; WCA: Water contact angle; $W_f$: Weight fraction of inorganic fillers; $X_c$: Degree of crystallinity.

## Supplementary Information

The online version contains supplementary material available at https://doi.org/10.1186/s42252-022-00029-5.

**Additional file 1.**

#### Acknowledgements

The authors acknowledge the support from Mrs. Sylvie Otis from Be-Up Biotechnology Inc. for providing P(HB-*co*-HV) samples, and Mrs. Caroline Potvin (UQAC) for her support in running the FTIR and DSC analyses.

#### Authors' contributions

SR contributed in the design of experiments and conceptualization of this current study, the acquisition of data and drafting of the manuscript. RJ contributed with his expert insights during the data analysis, data interpretation and revision of the manuscript. GM assisted with her intellectual input in related surface chemistry and morphology studies and gave a critical assessment in the final revision of the manuscript. All authors have read and agree with the final manuscript.

#### Funding

The authors appreciate the funding support from Natural Sciences and Engineering Research Council (NSERC), Canada.

#### Availability of data and materials

All data generated or analysed during this study are included in this published article. Any additional information on the available datasets used and/or analysed during the current study can be directed to the corresponding author on reasonable request.

## Declarations

#### Competing interests

The authors declare that they have no competing interests.

Received: 19 September 2021 Accepted: 4 January 2022
Published online: 24 February 2022

#### References

1. S. Wang, K. Liu, X. Yao, L. Jiang, Bioinspired Surfaces with Superwettability: New Insight on Theory, Design, and Applications. Chem. Rev. **115**, 8230–8293 (2015). https://doi.org/10.1021/cr400083y
2. M.G. Arshad, M. Farzaneh, A. Nekahi, Properties and applications of superhydrophobic coatings in high voltage outdoor insulation: A review. IEEE Trans. Dielectr. Electr. Insul. **24**, 3630–3646 (2017). https://doi.org/10.1109/TDEI.2017.006725
3. Z. Guo, F. Yang, *Surfaces and interfaces of biomimetic superhydrophobic materials* 1st. (Wiley-VCH, Weinheim, 2017)
4. R. Jafari, C. Cloutier, A. Allahdini, G. Momen, Recent progress and challenges with 3D printing of patterned hydrophobic and superhydrophobic surfaces. The International Journal of Advanced Manufacturing Technology **103**, 1225–1238 (2019). https://doi.org/10.1007/s00170-019-03630-4
5. K. Maghsoudi, E. Vazirinasab, G. Momen, R. Jafari, Advances in the Fabrication of Superhydrophobic Polymeric Surfaces by Polymer Molding Processes. Ind. Eng. Chem. Res. **59**, 9343–9363 (2020). https://doi.org/10.1021/acs.iecr.0c00508
6. G. Momen, M. Farzaneh, A ZnO-based nanocomposite coating with ultra water repellent properties. Appl. Surf. Sci. **258**, 5723–5728 (2012). https://doi.org/10.1016/j.apsusc.2012.02.074
7. E. Vazirinasab, R. Jafari, G. Momen, Application of superhydrophobic coatings as a corrosion barrier: A review. Surf. Coat. Technol. **341**, 40–56 (2018). https://doi.org/10.1016/j.surfcoat.2017.11.053
8. E. Vazirinasab, G. Momen, R. Jafari, A non-fluorinated mechanochemically robust volumetric superhydrophobic nanocomposite. J. Mater. Sci. Technol. **66**, 213–225 (2021). https://doi.org/10.1016/j.jmst.2020.06.029
9. A. Azimi Yancheshme, G. Momen, R. Jafari Aminabadi, Mechanisms of ice formation and propagation on superhydrophobic surfaces: A review. Adv. Colloid Interface Sci. **279**, 102155 (2020). https://doi.org/10.1016/j.cis.2020.102155
10. G. Rohman, *Biodegradable Polymers: Recent Developments and New Perspectives* (IAPC Publishing, Zagreb, Croatia, 2017)
11. Sindhu R, Binod P, Pandey A (2015) Microbial Poly-3-Hydroxybutyrate and Related Copolymers. In: Industrial Biorefineries & White Biotechnology. Elsevier, pp 575–605. https://doi.org/10.1016/B978-0-444-63453-5.00019-7
12. Rudnik E (2013) Biodegradability Testing of Compostable Polymer Materials. In: Handbook of Biopolymers and Biodegradable Plastics. Elsevier, pp 213–263. https://doi.org/10.1016/B978-1-4557-2834-3.00011-2

13. W. Yu, C.-H. Lan, S.-J. Wang, P.-F. Fang, Y.-M. Sun, Influence of zinc oxide nanoparticles on the crystallization behavior of electrospun poly(3-hydroxybutyrate-co-3-hydroxyvalerate) nanofibers. Polymer. **51**, 2403–2409 (2010). https://doi.org/10.1016/j.polymer.2010.03.024
14. C. Shuai, C. Wang, F. Qi, S. Peng, W. Yang et al., Enhanced Crystallinity and Antibacterial of PHBV Scaffolds Incorporated with Zinc Oxide. J. Nanomater. 2020, 1–12 (2020). https://doi.org/10.1155/2020/6014816
15. S. Vidhate, L. Innocentini-Mei, N.A. D'Souza, Mechanical and electrical multifunctional poly(3-hydroxybutyrate-co-3-hydroxyvalerate)-multiwall carbon nanotube nanocomposites. Polym. Eng. Sci. **52**, 1367–1374 (2012). https://doi.org/10.1002/pen.23084
16. A.P. Lemes, TLd.A. Montanheiro, A.P. Da Silva, N. Durán, PHBV/MWCNT Films: Hydrophobicity, Thermal and Mechanical Properties as a Function of MWCNT Concentration. Journal of Composites Science **3**, 12 (2019). https://doi.org/10.3390/jcs3010012
17. H.-Y. Yu, J.-M. Yao, Z.-Y. Qin, L. Liu, X.-G. Yang, Comparison of covalent and noncovalent interactions of carbon nanotubes on the crystallization behavior and thermal properties of poly(3-hydroxybutyrate- co -3-hydroxyvalerate). J. Appl. Polym. Sci. **130**, 4299–4307 (2013). https://doi.org/10.1002/app.39529
18. L.S. Montagna, TLd.A. Montanheiro, M.R. Baldan, A.P.S. Oliveira, M.A. de Farias et al., Effect of graphite nanosheets on electrical, electromagnetic, mechanical and morphological characteristics of PHBV/GNS nanocomposites. Adv. Mater. Lett. **9**, 499–504 (2018). https://doi.org/10.5185/amlett.2018.2044
19. V. Sridhar, I. Lee, H.H. Chun, H. Park, Graphene reinforced biodegradable poly(3-hydroxybutyrate-co-4-hydroxybutyrate) nano-composites. Express Polym Lett **7**, 320–328 (2013). https://doi.org/10.3144/expresspolymlett.2013.29
20. N.F. Braga, D.A. Vital, L.M. Guerrini, A.P. Lemes, D.M.D. Formaggio et al., PHBV-TiO2 mats prepared by electrospinning technique: Physico-chemical properties and cytocompatibility. Biopolymers **109**, e23120 (2018). https://doi.org/10.1002/bip.23120
21. Y. Xu, L. Zou, H. Lu, Y. Wei, J. Hua et al., Preparation and characterization of electrospun PHBV/PEO mats: The role of solvent and PEO component. J. Mater. Sci. **51**, 5695–5711 (2016). https://doi.org/10.1007/s10853-016-9872-0
22. M. Jafarpour, A.S. Aghdam, A. Koşar, F.Ç. Cebeci, M. Ghorbani, Electrospinning of ternary composite of PMMA-PEG-SiO2 nanoparticles: Comprehensive process optimization and electrospun properties. Materials Today Communications **29**, 102865 (2021). https://doi.org/10.1016/j.mtcomm.2021.102865
23. S. Sriram, A. Kumar, Separation of oil-water via porous PMMA/SiO2 nanoparticles superhydrophobic surface. Colloids Surf., A **563**, 271–279 (2019). https://doi.org/10.1016/j.colsurfa.2018.12.017
24. W. Qing, X. Li, Y. Wu, S. Shao, H. Guo et al., In situ silica growth for superhydrophilic-underwater superoleophobic Silica/PVA nanofibrous membrane for gravity-driven oil-in-water emulsion separation. J. Membr. Sci. **612**, 118476 (2020). https://doi.org/10.1016/j.memsci.2020.118476
25. L. Ji, X. Zhang, Ultrafine polyacrylonitrile/silica composite fibers via electrospinning. Mater. Lett. **62**, 2161–2164 (2008). https://doi.org/10.1016/j.matlet.2007.11.051
26. T.E. Newsome, S.V. Olesi. Electrospinning silica/polyvinylpyrrolidone composite nanofibers. J Appl Polym Sci **131**, (2014). https://doi.org/10.1002/app.40966
27. J. Seyfi, I. Hejazi, S.H. Jafari, H.A. Khonakdar, F. Simon, Enhanced hydrophobicity of polyurethane via non-solvent induced surface aggregation of silica nanoparticles. J Colloid Interface Sci **478**, 117–126 (2016). https://doi.org/10.1016/j.jcis.2016.06.005
28. P.M. Ma, R.Y. Wang, S.F. Wang, Y. Zhang, Y.X. Zhang et al., Effects of fumed silica on the crystallization behavior and thermal properties of poly(hydroxybutyrate-co-hydroxyvalerate). J. Appl. Polym. Sci. **108**, 1770–1777 (2008). https://doi.org/10.1002/app.27577
29. N. Ojha, N. Das, Fabrication and characterization of biodegradable PHBV/SiO2 nanocomposite for thermo-mechanical and antibacterial applications in food packaging. IET Nanobiotechnol. **9**, 785–795 (2020). https://doi.org/10.1049/iet-nbt.2020.0066
30. L. Wang, Y. Guo, Y. Chen, T. Chen, S. Zhu et al., Enhanced Mechanical and Water Absorption Properties of Rice Husk-Derived Nano-$SiO_2$ Reinforced PHBV Composites. Polymers (Basel) **10**, 1022 (2018). https://doi.org/10.3390/polym10091022
31. R. Khankrua, S. Pivsa-Art, H. Hiroyuki, S. Suttiruengwong, Thermal and Mechanical Properties of Biodegradable Polyester/Silica Nanocomposites. Energy Procedia **34**, 705–713 (2013). https://doi.org/10.1016/j.egypro.2013.06.803
32. B. Melendez-Rodriguez, K.J. Figueroa-Lopez, A. Bernardos, R. Martínez-Máñez, L. Cabedo et al., Electrospun Antimicrobial Films of Poly(3-hydroxybutyrate-co-3-hydroxyvalerate) Containing Eugenol Essential Oil Encapsulated in Mesoporous Silica Nanoparticles. Nanomaterials (Basel) **9**, 227 (2019). https://doi.org/10.3390/nano9020227
33. H. Nosal, K. Moser, M. Warzała, A. Holzer, D. Stańczyk et al., Selected Fatty Acids Esters as Potential PHB-V Bioplasticizers: Effect on Mechanical Properties of the Polymer. J. Polym. Environ. **29**, 38–53 (2020). https://doi.org/10.1007/s10924-020-01841-5
34. R. Requena, A. Jiménez, M. Vargas, A. Chiralt, Effect of plasticizers on thermal and physical properties of compression-moulded poly[(3-hydroxybutyrate)-co-(3-hydroxyvalerate)] films. Polym. Testing **56**, 45–53 (2016). https://doi.org/10.1016/j.polymertesting.2016.09.022
35. Wadey BL (2003) Plasticizers. In: Encyclopedia of Physical Science and Technology. Elsevier, pp 441–456. https://doi.org/10.1016/B0-12-227410-5/00586-X
36. V. Jost, H.-C. Langowski, Effect of different plasticisers on the mechanical and barrier properties of extruded cast PHBV films. Eur. Polymer J. **68**, 302–312 (2015). https://doi.org/10.1016/j.eurpolymj.2015.04.012
37. D. Lukáš, A. Sarkar, L. Martinová, K. Vodsed'álková, D. Lubasová et al., Physical principles of electrospinning (Electrospinning as a nano-scale technology of the twenty-first century). Text. Prog. **41**, 59–140 (2009). https://doi.org/10.1080/00405160902904641
38. I. Sas, R.E. Gorga, J.A. Joines, K.A. Thoney, Literature review on superhydrophobic self-cleaning surfaces produced by electrospinning. J. Polym. Sci., Part B: Polym. Phys. **50**, 824–845 (2012). https://doi.org/10.1002/polb.23070
39. H. Rodríguez-Tobías, G. Morales, D. Grande, Comprehensive review on electrospinning techniques as versatile approaches toward antimicrobial biopolymeric composite fibers. Mater Sci Eng C Mater Biol Appl **101**, 306–322 (2019). https://doi.org/10.1016/j.msec.2019.03.099
40. S. Ramakrishna, K. Fujihara, W.-E. Teo, T. Yong, Z. Ma et al., Electrospun nanofibers: solving global issues. Mater. Today **9**, 40–50 (2006). https://doi.org/10.1016/S1369-7021(06)71389-X
41. N. Nuraje, W.S. Khan, Y. Lei, M. Ceylan, R. Asmatulu, Superhydrophobic electrospun nanofibers. Journal of Materials Chemistry A **1**, 1929–1946 (2013). https://doi.org/10.1039/c2ta00189f
42. A. Pich, N. Schiemenz, C. Corten, H.-J.P. Adler, Preparation of poly(3-hydroxybutyrate-co-3-hydroxyvalerate) (PHBV) particles in O/W emulsion. Polymer **47**, 1912–1920 (2006). https://doi.org/10.1016/j.polymer.2006.01.038
43. M. Zhu, W. Zuo, H. Yu, W. Yang, Y. Chen, Superhydrophobic surface directly created by electrospinning based on hydrophilic material. J. Mater. Sci. **41**, 3793–3797 (2006). https://doi.org/10.1007/s10853-005-5910-z
44. B. Melendez-Rodriguez, J.L. Castro-Mayorga, M.A.M. Reis, C. Sammon, L. Cabedo et al., Preparation and Characterization of Electrospun Food Biopackaging Films of Poly(3-hydroxybutyrate-co-3-hydroxyvalerate) Derived From Fruit Pulp Biowaste. Frontiers in Sustainable Food Systems **2**, 38 (2018). https://doi.org/10.3389/fsufs.2018.00038
45. D.-G. Yu, W.-C. Lin, C.-H. Lin, M.-C. Yang, Cytocompatibility and antibacterial activity of a PHBV membrane with surface-immobilized water-soluble chitosan and chondroitin-6-sulfate. Macromol Biosci **6**, 348–357 (2006). https://doi.org/10.1002/mabi.200600026
46. A. Wang, Y. Gan, H. Yu, Y. Liu, M. Zhang et al., Improvement of the cytocompatibility of electrospun poly(R)-3-hydroxybutyrate-co-(R)-3-hydroxyvalerate mats by Ecoflex. J Biomed Mater Res A **100**, 1505–1511 (2012). https://doi.org/10.1002/jbm.a.34034
47. C.N. Degeratu, G. Mabilleau, E. Aguado, R. Mallet, D. Chappard et al., Polyhydroxyalkanoate (PHBV) fibers obtained by a wet spinning method: Good in vitro cytocompatibility but absence of in vivo biocompatibility when used as a bone graft. Morphologie **103**, 94–102 (2019). https://doi.org/10.1016/j.morpho.2019.02.003
48. A. BalakrishnaPillai, A. Jaya Kumar, H. Kumarapillai, Biosynthesis of poly(3-hydroxybutyrate-co-3-hydroxyvalerate) (PHBV) in Bacillus aryabhattai and cytotoxicity evaluation of PHBV/poly(ethylene glycol) blends. 3 Biotech **10**, 32 (2020). https://doi.org/10.1007/s13205-019-2017-9
49. X. Zhao, Y. Liu, C. Wang, Q. Liu, Structure and filtration performance of fibrous composite membranes containing environmentally friendly

materials for water purification. Fibers and Polymers **16**, 2586–2592 (2015). https://doi.org/10.1007/s12221-015-5562-9
50. D. Grande, J. Ramier, D.L. Versace, E. Renard, V. Langlois, Design of functionalized biodegradable PHA-based electrospun scaffolds meant for tissue engineering applications. N Biotechnol **37**, 129–137 (2017). https://doi.org/10.1016/j.nbt.2016.05.006
51. Y. Xu, L. Zou, H. Lu, T. Kang, Effect of different solvent systems on PHBV/PEO electrospun fibers. RSC Adv. **7**, 4000–4010 (2017). https://doi.org/10.1039/c6ra26783a
52. Y. Li, W. Weng, Surface modification of hydroxyapatite by stearic acid: characterization and in vitro behaviors. J Mater Sci Mater Med **19**, 19–25 (2008). https://doi.org/10.1007/s10856-007-3123-5
53. L. Feng, H. Zhang, P. Mao, Y. Wang, Y. Ge, Superhydrophobic alumina surface based on stearic acid modification. Appl. Surf. Sci. **257**, 3959–3963 (2011). https://doi.org/10.1016/j.apsusc.2010.11.143
54. Mojiri H, Aliofkhazraei M (2017) 3.19 Effect of Surface Roughness on Wetting Properties. In: Comprehensive Materials Finishing. Elsevier, pp 276–305. https://doi.org/10.1016/B978-0-12-803581-8.09181-5
55. C.H. Chan, C. Kummerlöwe, H.-W. Kammer, Crystallization and Melting Behavior of Poly(3-hydroxybutyrate)-Based Blends. Macromol. Chem. Phys. **205**, 664–675 (2004). https://doi.org/10.1002/macp.200300062
56. Y.I. Yoon, H.S. Moon, W.S. Lyoo, T.S. Lee, W.H. Park, Superhydrophobicity of PHBV fibrous surface with bead-on-string structure. J Colloid Interface Sci **320**, 91–95 (2008). https://doi.org/10.1016/j.jcis.2008.01.029
57. H.W. Tong, M. Wang, Effects of Processing Parameters on the Morphology and Size of Electrospun PHBV Micro- and Nano-Fibers. Key Eng. Mater. **334–335**, 1233–1236 (2007). https://doi.org/10.4028/www.scientific.net/KEM.334-335.1233
58. S. Liu, D. Li, Y. Yang, L. Jiang, Fabrication, mechanical properties and failure mechanism of random and aligned nanofiber membrane with different parameters. Nanotechnol. Rev. **8**, 218–226 (2019). https://doi.org/10.1515/ntrev-2019-0020
59. S. Huan, G. Liu, G. Han, W. Cheng, Z. Fu et al., Effect of Experimental Parameters on Morphological, Mechanical and Hydrophobic Properties of Electrospun Polystyrene Fibers. Materials **8**, 2718–2734 (2015). https://doi.org/10.3390/ma8052718
60. S.J. Upson, T. O'Haire, S.J. Russell, K. Dalgarno, A.M. Ferreira, Centrifugally spun PHBV micro and nanofibres. Mater Sci Eng C Mater Biol Appl **76**, 190–195 (2017). https://doi.org/10.1016/j.msec.2017.03.101
61. A. Haider, S. Haider, I.-K. Kang, A comprehensive review summarizing the effect of electrospinning parameters and potential applications of nanofibers in biomedical and biotechnology. Arab. J. Chem. **11**, 1165–1188 (2018). https://doi.org/10.1016/j.arabjc.2015.11.015
62. I.T. Seoane, L.B. Manfredi, V.P. Cyras, Effect of two different plasticizers on the properties of poly(3-hydroxybutyrate) binary and ternary blends. J. Appl. Polym. Sci. **135**, 46016 (2018). https://doi.org/10.1002/app.46016
63. C. Wang, C. Piao, From hydrophilicity to hydrophobicity: A critical review-part II: Hydrophobic conversion. Wood Fiber Sci. **43**, 41–56 (2011)

## Publisher's Note